

Near room temperature antiferromagnetic ordering with a potential low dimensional magnetism in AlMn_2B_2

Tej N. Lamichhane,¹ Khusboo Rana,¹ Qisheng Lin,² Sergey L. Bud'ko,¹ Yuji Furukawa,¹ and Paul C. Canfield¹
¹Ames Laboratory, U.S. DOE, and Department of Physics and Astronomy, Iowa State University, Ames, Iowa 50011, USA
²Ames Laboratory, U.S. DOE and Department of Chemistry, Iowa State University, Ames, Iowa 50011, USA

We present self flux growth and characterization of single crystalline AlMn_2B_2 . It is an orthorhombic (space group Cmmm), layered material with a plate like morphology. The anisotropic bulk magnetization data, electrical transport and ^{11}B nuclear magnetic resonance(NMR) data revealed an antiferromagnetic (AFM) transition at 313 ± 2 K. In the magnetization data, there is also a broad local maximum significantly above the AFM transition that could be a signature of low dimensional magnetic interactions in AlMn_2B_2 .

INTRODUCTION

The AlT_2B_2 ($T = \text{Fe}, \text{Cr}, \text{Mn}$) system crystallizes in the orthorhombic, Cmmm structure and adopts a layer morphology with an internal structure of alternate stacking of Al atom planes and T_2B_2 slabs along the b -axis [1]. A representative unit cell of AlMn_2B_2 is shown in Fig. 1(a) to demonstrate this atomic structure. AlT_2B_2 compounds are interesting, specially for potential rare earth free magnetocaloric materials and soft magnetic materials. AlFe_2B_2 is ferromagnetic and studied for its magneto-caloric and anisotropic magnetic properties [2–4]. Understanding the magnetic properties of the neighbouring, isostructural compounds can provide further insight in to the series as well as how to tune the magnetocaloric property of the AlFe_2B_2 via substitution. We started this work to clarify the magnetic properties of AlMn_2B_2 since it was identified as a non-magnetic material [5]. In addition, some inconsistencies between bulk and local probe magnetic measurements in the $\text{Al}(\text{Fe}_{1-x}\text{Mn}_x)_2\text{B}_2$ were observed. A later first principle calculation suggested that AlMn_2B_2 should be an anti-ferromagnetic compound [6]. In a recent powder neutron study, AlMn_2B_2 is identified as a ceramic AFM compound [7] with Neel temperature around 390 K. A study of lattice parameters variation from room temperature to 1200 K revealed that there is a change in anisotropy nature in a and c lattice parameters around 450 K and a local minimum in b lattice parameters around 400 K [8]. The lack of a clear description of the nature or number of magnetic phase transitions in AlMn_2B_2 led us to grow and systematically study single crystalline samples.

This paper reports the synthesis of bulk single crystals via high-temperature solution growth and their characterization via high and low temperature magnetization, NMR, and electrical resistance measurements. We find that AlMn_2B_2 is a metallic antiferromagnet with a transition temperature of $T_N = 313 \pm 2$ K. In addition we find that AlMn_2B_2 has features associated with pseudo-two-dimensional magnets.

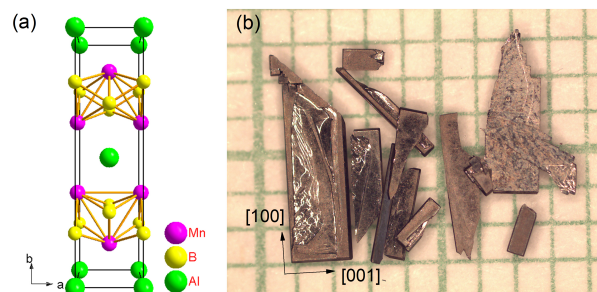


FIG. 1. (a) AlMn_2B_2 unit cell showing Mn_2B_2 slabs stacked with Al layer (b) Concentrated NaOH etched AlMn_2B_2 single crystals

EXPERIMENTAL DETAILS

Crystal growth

Solution growth is a powerful tool even for compounds with high melting elements like B [3, 9, 10]. The major difficulty associated with solution growth is finding an initial composition that allows for growth of the single phase, desired compound. For example, $\text{CaKFe}_4\text{As}_4$ growth in single phase form presents an illustrative example [11]. Fortunately, with the innovation of fritted alumina crucibles sets [12] we can now reuse decanted melt and essentially fractionate the melt, as described below.

Al shot (Alfa Aesar 99.999%), B pieces (Alfa Aesar 99.5% metal basis) and Mn pieces (Alfa Aesar 99.9% metal basis) after surface oxidation cleaning as described elsewhere [13] were used for the crystal growth process. We started with an Al rich composition, $\text{Al}_{68}\text{Mn}_{22}\text{B}_{10}$, and arc-melted it at least 4 times under an Ar atmosphere. The button was then cut with a metal cutter and re-arc-melted if some not-reacted B pieces were found. After the button appeared to be homogeneous, it was packed in a fritted alumina crucible set [12] and sealed under partial pressure of argon inside amorphous silica jacket to form a growth ampoule. The growth ampoule

TABLE I. Crystal data and structure refinement for AlMn_2B_2 .

Empirical formula	AlMn_2B_2
Formula weight	158.48
Temperature	296(2) K
Wavelength	0.71073 Å
Crystal system, space group	Orthorhombic, $Cmmm$
Unit cell dimensions	a=2.9215(1) Å b = 11.0709(6) Å c = 2.8972(2) Å
Volume	$93.706(9) \times 10^3 \text{ Å}^3$
Z, Calculated density	2, 5.63 g/cm ³
Absorption coefficient	6.704 mm ⁻¹
F(000)	73
θ range (°)	3.693 to 29.003
Limiting indices	$-5 \leq h \leq 5$ $-22 \leq k \leq 22$ $-5 \leq l \leq 5$
Reflections collected	1467
Independent reflections	270 [R(int) = 0.0401]
Completeness to $\theta = 25.242^\circ$	98.5%
Absorption correction	multi-scan, empirical
Refinement method	Full-matrix least-squares
Data / restraints / parameters	270 / 0 / 12
Goodness-of-fit on F^2	1.101
Final R indices [$I > 2\sigma(I)$]	$R1 = 0.0362$, $wR2 = 0.0817$
R indices (all data)	$R1 = 0.0387$, $wR2 = 0.0824$
Largest diff. peak and hole	2.341 and -1.249 e.Å ⁻³

TABLE II. Atomic coordinates and equivalent isotropic displacement parameters (Å^2) for AlMn_2B_2 . U_{eq} is defined as one third of the trace of the orthogonalized U_{ij} tensor.

atom	Wyckoff site	x	y	z	U_{eq}
Mn	$4j$	0	0.3552(1)	1/2	0.0070(1)
Al	$2a$	0	0	0	0.0067(5)
B	$4i$	0	0.2065(5)	0	0.0070(1)

was then heated to 1200 °C over 2 h and soaked there for 10 h before spinning using a centrifuge. Due to high melting point of B containing compounds, homogeneous liquid was not formed at 1200 °C. Undissolved polycrystalline MnB and Al-Mn binary compounds were separated at 1200 °C via centrifuging. The catch crucible collected the homogeneous melt at 1200 °C was again sealed in a fritted alumina crucible sets under Ar atmosphere to form second growth ampoule. This second ampoule was heated to 1200 °C over 2 h, held there for another 10 h and cooled down to 1100 °C over 50 h and spun using

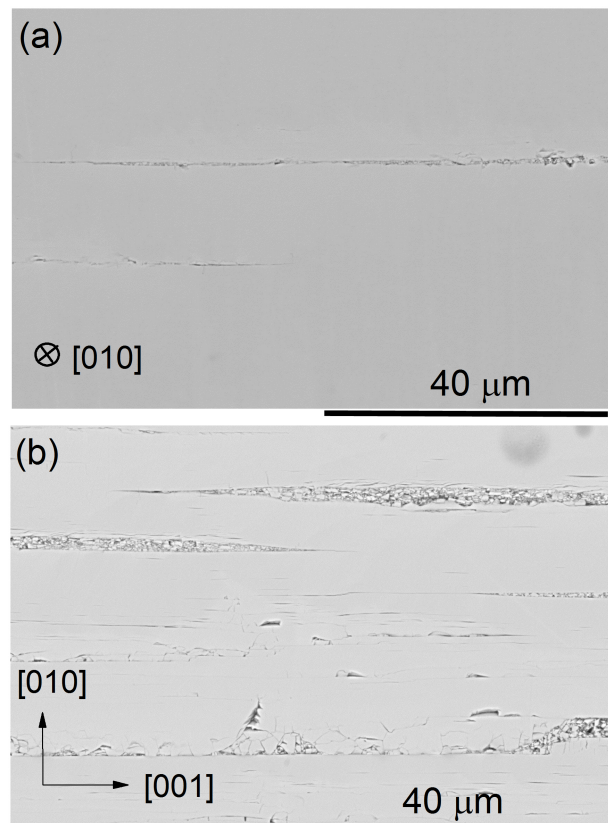


FIG. 2. (a) SEM image of AlMn_2B_2 single crystalline sample along the planar view (with electron beam parallel to $[010]$) (b) SEM image of AlMn_2B_2 in a cross sectional view with electron beam parallel to $[100]$.

centrifuge to separate the crystals. The second growth attempt produced a mixture of the targeted AlMn_2B_2 phase along with MnB crystals. So as to avoid this MnB contamination, the catch crucible of the second growth was used for a third growth and sealed again under a partial pressure of Ar. For this stage, to make sure there are no other nucleated crystals, the third growth growth was heated to 1200 °C over 2 h and soaked there for 2 h. It was then cooled down to 1100 °C over 1 h and stayed there for 1 h followed by slow cooling to 990 °C over 120 h and centrifuged to separate large, single phased AlMn_2B_2 crystals as shown in Fig. 1(b). The flux on the surface was removed via concentrated NaOH etching.

It should be noted that predominantly single phase AlMn_2B_2 crystals were grown in single growth attempt using initial $\text{Al}_{84}\text{Mn}_8\text{B}_8$ composition however the crystals were small, due to multiple nucleation sites.

CRYSTAL STRUCTURE AND STOICHIOMETRY

As grown single crystals were characterized using a scanning electron microscope (SEM), as well as both

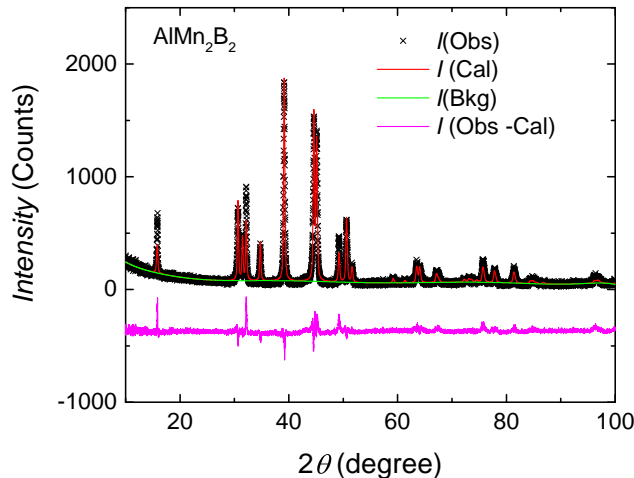


FIG. 3. Single crystal crushed powder XRD pattern where I (Obs), I (Cal), I (Bkg) and I (Obs-Cal) are observed, calculated, background and differential diffractograms respectively.

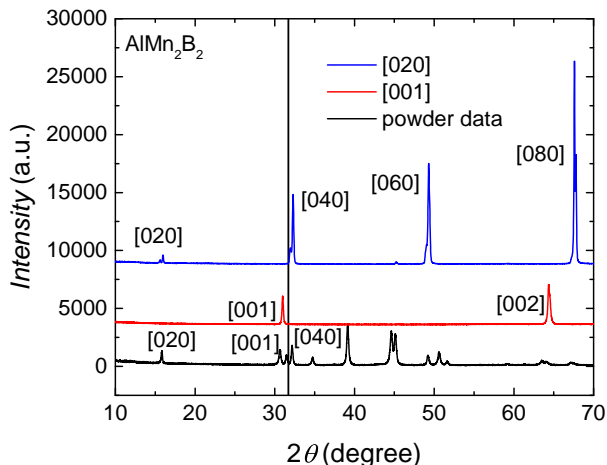


FIG. 4. Crystallographic orientation characterization of AlMn_2B_2 surfaces using monochromatic $\text{Cu } K_\alpha$ radiation in Bragg Brentano diffraction geometry. The top curve shows the family of $\{020\}$ peaks identifying direction perpendicular to plate as $[010]$. The direction along the thickness of the plates is found to be $[001]$ leaving the direction along the length as $[100]$. The vertical grid line through the $[110]$ powder diffraction peak (not labeled in diagram) is a reference to identify $[001]$ and $[040]$ peaks observed for different facets.

powder and single crystal X-ray diffraction (XRD). Figures 2(a) and (b) show the planar and cross sectional backscattered SEM images of AlMn_2B_2 single crystals which show predominantly homogeneous compositions. The small linear grooves are the cracked layers associated with the SEM sample polishing. Being a layered

material, it can be easily cleaved and deformed. Boron is difficult to account for correctly in electron dispersive spectroscopy (EDS), as a consequence of this we determined only the Mn:Al ratio for two different batches of single crystalline samples. In first batch, 13 spots were analyzed in EDS with Mn:Al ratio of 2.07 for all characteristics X-ray emissions. Similarly, an 8 spot analysis in the second batch provided the Mn:Al ratio to be 2.12 for characteristics K -lines for all elements. With the L -characteristics-lines analysis, a ratio of 2.51 was obtained for the second batch. Without the creation and use of Mn-Al-B based standards, further characterization by EDS is difficult.

Although the EDS results are qualitatively in agreement with the AlMn_2B_2 structure, to more precisely determine the composition and structure, multiple batches of AlMn_2B_2 were investigated using single crystal XRD technique. Single crystalline XRD data were collected with the use of graphite monochromatized $\text{Mo } K_\alpha$ radiation ($\lambda=0.71073 \text{ \AA}$) at room temperature on a Bruker APEX2 diffractometer. Reflections were gathered by taking five sets of 440 frames with 0.5° scans in ω/θ , with an exposure time of 10 s per frame and the crystal-to-detector distance of 6 cm. The structure solution and refinement for single crystal data was carried out using SHELXTL program package. Attempts to refine occupancies of each site indicated full occupancy ($< 3\sigma$). The final stage of refinement was performed using anisotropic displacement parameters for all the atoms. The refinement metrics and atomic coordinates are presented in TABLE I and II respectively. The single crystalline refinement showed AlMn_2B_2 as a stoichiometric material.

Etched single crystals were finely ground and spread over a zero background silicon wafer sample holder with help of a thin film of Dow Corning high vacuum grease. Powder diffraction data were obtained using a Rigaku Miniflex II diffractometer within a 2θ range of $10 - 100^\circ$ with a step of 0.02° and dwelling time of 3 seconds for data acquisition. The crystallographic information file from the single crystal XRD solution was used to fit the powder XRD data using GSAS [14] and EXPGUI [15] software packages. Figure 3 shows the Rietveld refined powder XRD pattern with R factor of 0.08. Being a relatively hard, layered material, texture is visible along $[020]$ direction although March Dollase texture correction was employed to account for this intensity mismatch.

To identify the crystallographic orientation of the AlMn_2B_2 single crystals, we employed the monochromatic X-ray diffraction from the crystallographic surfaces in the Bragg-Brentano geometry [3, 16]. The direction perpendicular to the plate was identified to be $[010]$ since a family of $\{020\}$ lines were observed in the diffraction pattern as shown in blue curve in Fig. 4. The plate was held vertical and the family of $\{001\}$ peaks were obtained as shown in red curve of Fig. 4. The monochromatic x-ray surface diffraction peaks were compared with powder

diffraction data to correctly identify their directions. A vertical line through the powder [110] peak was used as a reference point of comparison as shown in Fig. 4. Then the last remaining direction was identified to be [100] along the length of the crystals. A reference coordinate system is shown in Fig. 1(b) to demonstrate the crystallographic orientations of AlMn_2B_2 crystals.

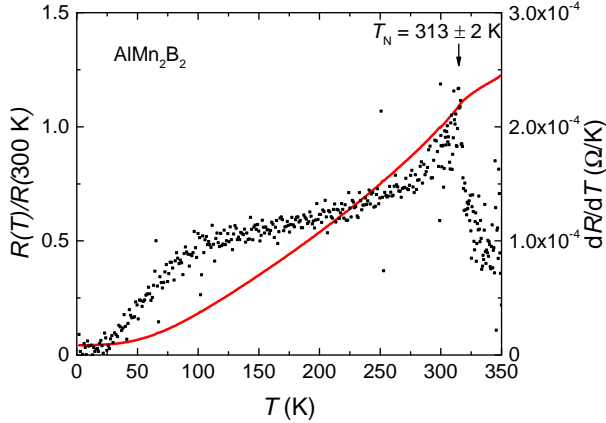


FIG. 5. Temperature dependent normalized resistance (left axis) and temperature derivative (right axis) of AlMn_2B_2 . The resistance is metallic in nature. The temperature derivative shows an anomaly at 313 ± 2 K consistent with an AFM phase transition.

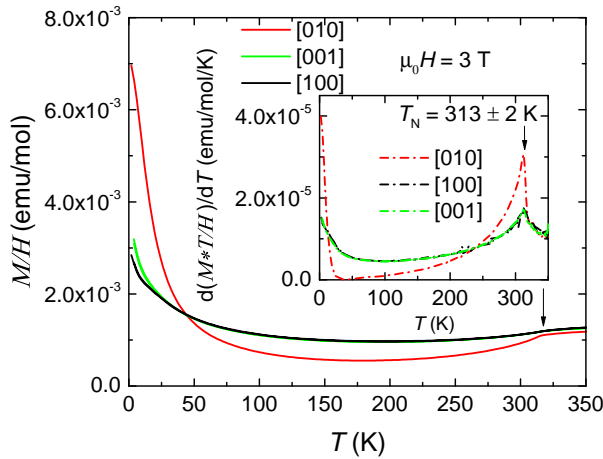


FIG. 6. Low temperature (2 - 350 K) M/H along various crystallographic axes of AlMn_2B_2 sample as outlined in the graph. The inset shows $\frac{d(M*T/H)}{dT}$ as a function of temperature.

ELECTRIC AND MAGNETIC PROPERTIES

The temperature dependent electrical resistance of AlMn_2B_2 was measured in a traditional 4 probe measurement on a NaOH etched, rod like sample using an

external device control option to interface with a Linear Research, Inc. ac (1 mA, 17 Hz) resistance bridge (LR 700). Thin platinum wires were attached to the sample using DuPont 4929N silver paint to make electrical contact. Quantum Design Magnetic Property Measurement System (MPMS) was used as a temperature controller. The measured temperature dependent electrical resistance of AlMn_2B_2 is shown in Fig. 5. These data further confirm that our single crystals are essentially stoichiometric AlMn_2B_2 ; given that the residual resistivity ratio ($\frac{R(350.0\text{K})}{R(2.0\text{K})}$) is 28.5, there is relatively low disorder scattering. In addition, a very clear feature is seen in both $R(T)$ and $\frac{d(R(T))}{dT}$ at $T = 313 \pm 2$ K. Such features are often related to a loss of spin disorder scattering at a magnetic transition [17]. As such, these data are our first suggestion that AlMn_2B_2 may indeed have some form of magnetic order below 315 K.

The magnetic properties of AlMn_2B_2 were studied from a base temperature of 2 K to 700 K. Low temperature anisotropic magnetization data of single crystalline AlMn_2B_2 samples were measured within the temperature range 2 - 350 K using a MPMS. High temperature,

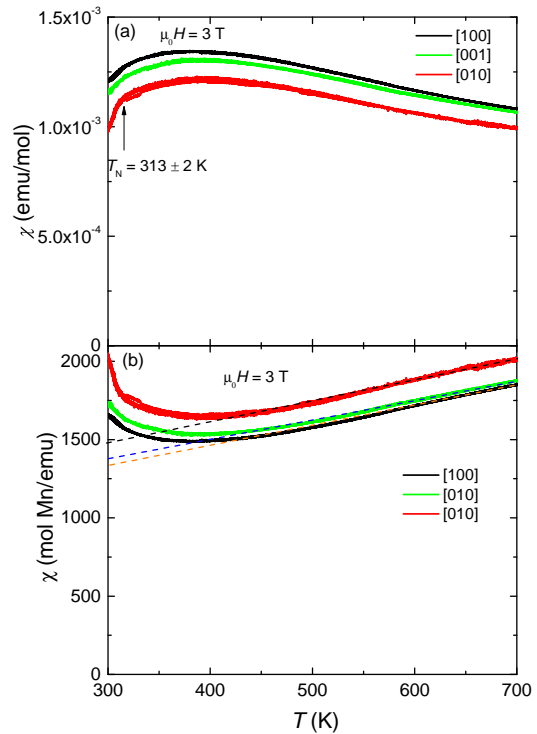


FIG. 7. (a) High temperature susceptibility data along various axes measured using VSM. There are shallow anomalies present around 313 ± 2 K for each directions. (b) Corresponding Curie Weiss plots identifying AlMn_2B_2 as an AFM material with $\theta_{010} = -815$ K, $\theta_{100} = -750$ K, and $\theta_{001} = -835$ K respectively.

anisotropic temperature dependent magnetization data were obtained using a Quantum Design VersaLab Vibrating Sample Magnetometer (VSM) over the temperature range 300 - 700 K in an oven option mode.

The low temperature anisotropic susceptibility data, with $H = 3$ T applied field, are presented in Fig. 6. Below 50 K, the magnetization data show a low temperature upturn as reported in a previous literature [5]. In all three directions, there is a clear anomaly in susceptibility data around 312 K. The inset shows $\frac{d(M*T/H)}{dT}$ as a function of temperature [18] showing a clear anomaly around 312 K identifying AlMn_2B_2 as a AFM material. The observed anomaly in $\frac{d(M*T/H)}{dT}$ coincides with the kink observed in $\frac{dR}{dT}$.

Recently, AlMn_2B_2 was reported to be AFM however Neel temperature was reported to be around 390 K [7]. To examine higher temperatures, our high temperature susceptibility data, obtained using our VSM are presented in Fig. 7(a) and (b). Although a broad local maximum of the susceptibility around 350 - 390 K for different axes, consistent to reference[7] was found, the $\frac{d(M*T/H)}{dT}$ did not show any anomaly. The only clear and conclusive feature in the high temperature data associated with a magnetic transition is the feature at 313 ± 2 K. The broad local maximum in magnetization well above the transition temperature can be associated with low dimensional, or linear chain anisotropic Heisenberg antiferromagnetism [19–23]. The fitted Curie Weiss temperatures for various axes were obtained to be $\theta_{010} = -$

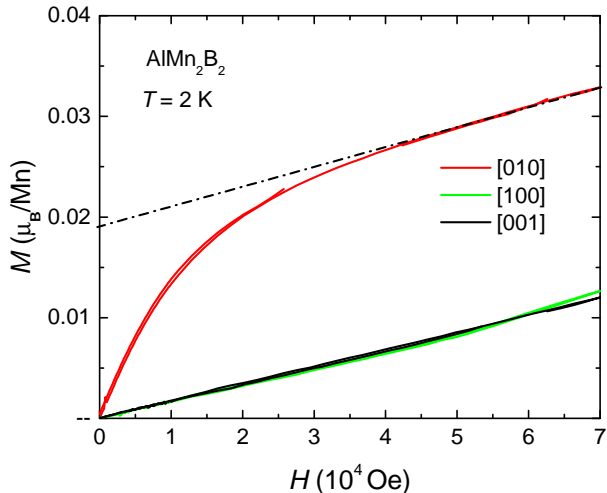


FIG. 8. Field dependent magnetization $M(H)$ of AlMn_2B_2 at 2 K. The magnetization along [010] direction shows a saturation magnetization of $0.02 \mu_B/\text{Mn}$ with respect to other two principle directions outlined with a linear fit of the high field region data. The $M(H)$ data along [010] direction shows no magnetic hysteresis i.e. the almost overlapping 2 red curves for increasing and decreasing field. The At higher field region, all 3 $M(H)$ data have the same slopes.

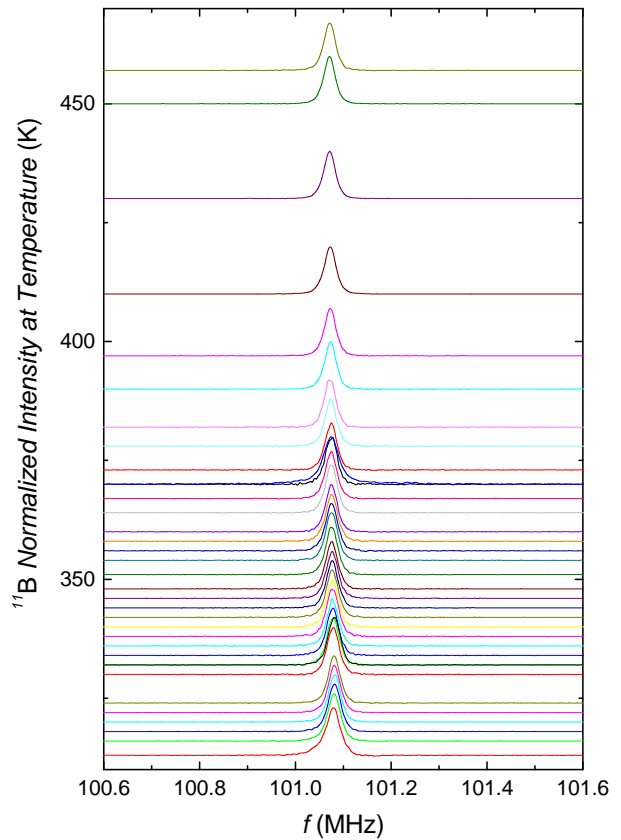


FIG. 9. ^{11}B NMR spectrum measured at different temperatures from 315 to 457 K with $H = 7.4089$ T.

815 K, $\theta_{100} = -750$ K, and $\theta_{001} = -835$ K. From the average slope of Curie Weiss plot, the effective moment of Mn is found to be $\sim 2.5 \mu_B/\text{Mn}$.

At low temperature, $T \leq 50$ K, in Fig. 6 there is a clear upturn in the M/H data, particularly for H along the [010] direction. In order to better understand this we measured the anisotropic field dependent magnetization at 2 K as shown in Fig. 8. For fields greater than 4 T the slopes of the $M(H)$ plots are comparable for all three directions. For $H \parallel [010]$, there is a roughly $0.02 \mu_B/\text{Mn}$ offset due to a rapid increase and saturation for $H \leq 3$ T. The origin of this small, anisotropic contribution is currently not known.

NUCLEAR MAGNETIC RESONANCE STUDY

To further investigate the magnetism of AlMn_2B_2 , we carried out ^{11}B NMR measurements at various temperatures between 5 K and 457 K as presented in Figs. 9 - 11. To perform the NMR measurements for the temperature region of $T = 5 - 295$ K, crushed single crystalline powder was enclosed in a weighing paper folded closed cylindrical tube and inserted inside the NMR coil.

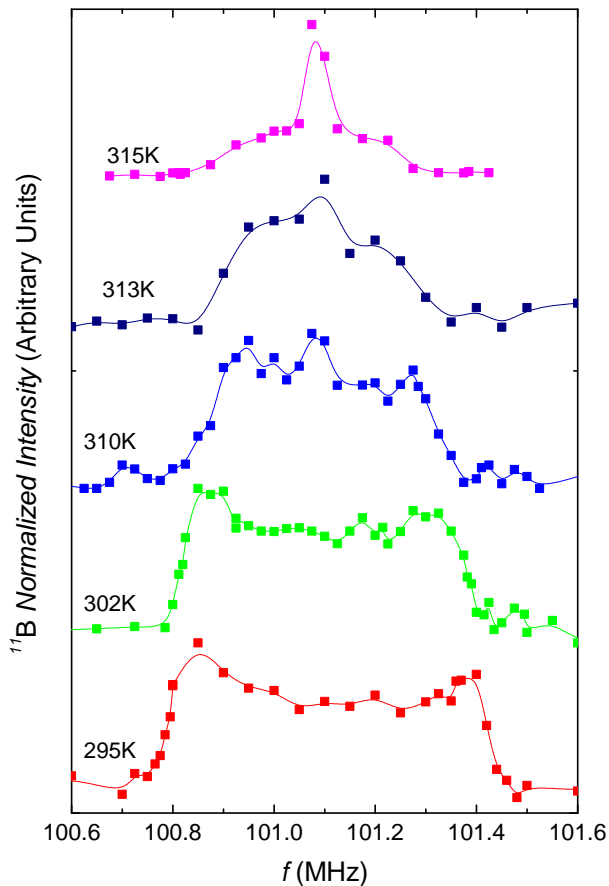


FIG. 10. ^{11}B NMR spectra measured at $H = 7.4089$ T by sweeping frequency.

For the higher temperature NMR measurements up to 457 K from room temperature, the crushed powder was sealed under $\frac{1}{3}$ atmospheric pressure of Ar inside a ~ 1 mm internal diameter amorphous silica tube. The NMR measurements were carried out using a lab-built phase coherent spin-echo pulsed NMR spectrometer on ^{11}B (nuclear spin $I = \frac{3}{2}$ and gyromagnetic ratio $\frac{\gamma_N}{2\pi} = 13.6552$ MHz/T) nuclei in the temperature range $5 < T < 457$ K. NMR spectra were obtained either by Fourier transform of the NMR echo signals, by sweeping frequency or by sweeping magnetic field. Magnetic phase transition was studied analyzing the full width at half maximum (FWHM) of ^{11}B NMR spectra and spin-lattice relaxation rate $\frac{1}{T_1}$. The ^{11}B $\frac{1}{T_1}$ was measured by the conventional single saturation pulse method.

Figure 9 shows the ^{11}B NMR spectra obtained by Fourier transform of the NMR spin echo for temperatures in the range 315 - 457 K at $H = 7.4089$ T. Throughout the range of study, the FWHM ~ 29 kHz is nearly independent of temperature. On the other hand, below 315 K, as shown in Fig. 10, the ^{11}B NMR line broadens abruptly and has an almost rectangular shape at low temperatures. Since the rectangular shape is character-

istic of NMR spectrum in AFM ordered state for powder sample, the results clearly indicate that the magnetic phase transition around 315 K is AFM. Similar rectangular NMR spectra in AFM state have been observed in BiMn_2PO_6 [24], NaVGe_2O_6 [25], CuV_2O_6 [26], and $\text{BaCo}_2\text{V}_2\text{O}_8$ [27].

In the low temperature range between 5 - 295 K, several ^{11}B NMR spectra were measured at a frequency of $f = 44.32$ MHz by sweeping the magnetic field as shown in Fig. 11. The FWHM increases with decreasing temperature and shows nearly constant (~ 0.06 T) down to ~ 50 K. Below 50 K, the FWHM slightly decreases, where the shape of the spectrum changes and the edges of the lines are smeared out. These results suggest a change in magnetic state around 50 K. Although it is not clear at present, it is interesting if the change relates to the strong enhancement of χ_b below 50 K as shown in Fig. 6. NMR measurements on single crystals could provide additional information in this issue. This is the future work.

Figure 12(a) shows the temperature variation of the FWHM of the ^{11}B NMR spectra between 5 - 457 K. Since the FWHM of the powder NMR spectrum in AFM state corresponds to the twice of the hyperfine field (H_{hf}) at the B site produced by Mn ordered moments, the temperature dependence of FWHM reflects the temperature dependence of the Mn sub-lattice magnetization. Therefore, one can obtain the critical exponent (β) of the order parameter using the formula $\text{FWHM} \propto (1 - \frac{T}{T_N})^\beta$. The maximum value of $\beta = 0.21 \pm 0.02$ with $T_N = 314$ K was obtained by fitting the data points in the range 295

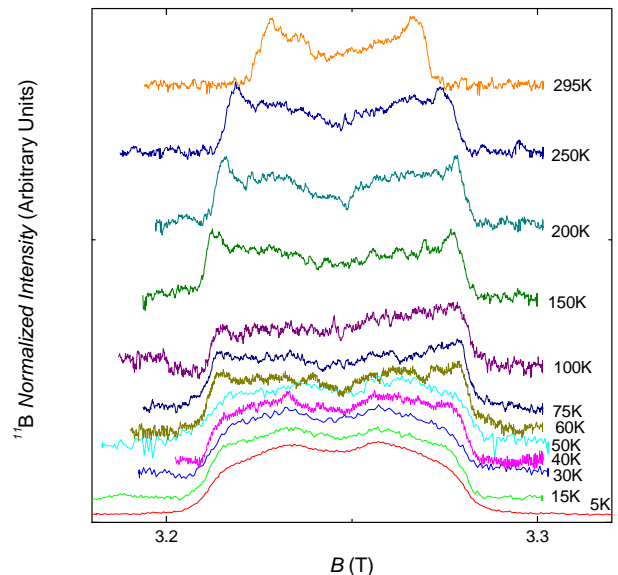


FIG. 11. ^{11}B NMR spectra measured at different temperatures between 5 K and 295 K measured using field sweeping method. A noticeable change in shape of ^{11}B NMR peaks around 50 K coincides with changing the magnetic anisotropy between $[100]/[001]$ and $[010]$ directions as shown in Fig. 6.

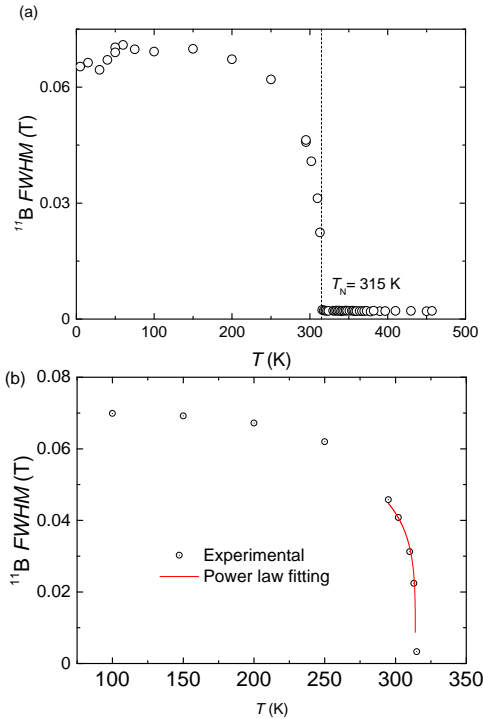


FIG. 12. (a) Temperature dependence of FWHM ^{11}B NMR spectra in powdered AlMn_2B_2 sample showing AFM transition around 315 K. (b) Power law fitting of the observed temperature variation of ^{11}B FWHM in the temperature range 295 - 315 K as $\text{FWHM} \propto [1 - (\frac{T}{T_N})]^\beta$ with $T_N = 314$ K and $\beta = 0.21 \pm 0.02$.

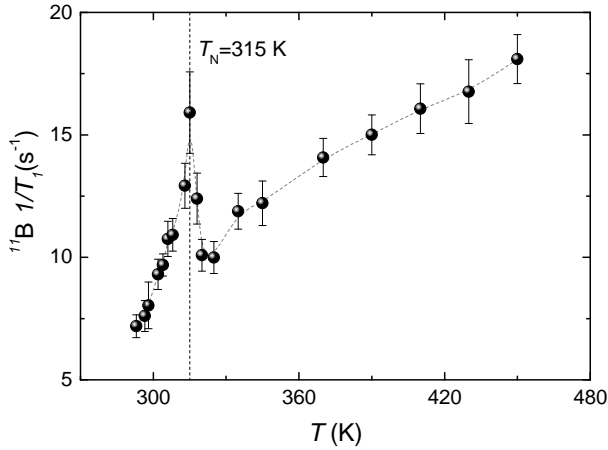


FIG. 13. The inverse of relaxation rate (T_1) is plotted as a function of T from 293 K to 450 K. The transition temperature at 315 K is evidenced by a sharp peak of $\frac{1}{T_1}$.

K - 315 K close to T_N as shown in Fig. 12(b). Very nominal change was observed in the fitted β parameter with the extension of fitted range toward the low tem-

perature. The observed change in critical exponent β was within the error bar for all the temperature range. This power law fittings of FWHM provided lower value of $\beta = 0.21 \pm 0.02$ (for 3D Heisenberg model $\beta \sim 0.345$) suggesting a low dimensional magnetism as discussed in reference[19].

To study the dynamical properties of the Mn spins in high temperature range, the spin lattice relaxation rates ($\frac{1}{T_1}$) at the ^{11}B site were measured from room temperature to 457 K. Figure 13 shows the temperature dependence of $\frac{1}{T_1}$ where $\frac{1}{T_1}$ shows a clear peak at 315 K, evidencing again the AFM ordering. On the other hand, no clear anomaly in the temperature dependence of $\frac{1}{T_1}$ is observed around 390 K where the magnetic susceptibility exhibits a broad local maximum. Therefore, the broad maximum in the magnetic susceptibility is not associated with a magnetic ordering, but it could be attributed to a two dimensional magnetic character in AlMn_2B_2 as observed in 2D AFM compounds such as $\text{BaMn}_2\text{Si}_2\text{O}_7$ [19].

CONCLUSIONS

Structural, electrical transport and magnetic properties were studied on self flux grown single crystalline AlMn_2B_2 samples. All these measurements revealed that AlMn_2B_2 as an AFM compound with a transition temperature around 313 ± 2 K. At higher temperature broad hump, well above the transition temperature, could be the signature of low dimensional magnetic interaction in AlMn_2B_2 above the room temperature.

ACKNOWLEDGEMENT

Dr. Warren Straszheim is acknowledged for doing SEM on various samples. This research was supported by the Critical Materials Institute, an Energy Innovation Hub funded by the U.S. Department of Energy, Office of Energy Efficiency and Renewable Energy, Advanced Manufacturing Office. This work was also supported by the office of Basic Energy Sciences, Materials Sciences Division, U.S. DOE. This work was performed at the Ames Laboratory, operated for DOE by Iowa State University under Contract No. DE-AC02-07CH11358.

-
- [1] Qianheng Du, Guofu Chen, Wenyun Yang, Jianzhong Wei, Muxin Hua, Honglin Du, Changsheng Wang, Shunquan Liu, Jingzhi Han, Yan Zhang, and Jinbo Yang, "Magnetic frustration and magnetocaloric effect in $\text{AlFe}_{2-x}\text{Mn}_x\text{B}_2$ ($x = 0-0.5$) ribbons," Journal of Physics D: Applied Physics **48**, 335001 (2015).

- [2] Xiaoyan Tan, Ping Chai, Corey M. Thompson, and Michael Shatruk, "Magnetocaloric Effect in AlFe_2B_2 : Toward Magnetic Refrigerants from Earth-Abundant Elements," *Journal of the American Chemical Society* **135**, 9553–9557 (2013), pMID: 23731263, <https://doi.org/10.1021/ja404107p>.
- [3] Tej N. Lamichhane, Li Xiang, Qisheng Lin, Tribhuwan Pandey, David S. Parker, Tae-Hoon Kim, Lin Zhou, Matthew J. Kramer, Sergey L. Bud'ko, and Paul C. Canfield, "Magnetic properties of single crystalline itinerant ferromagnet AlFe_2B_2 ," *Phys. Rev. Materials* **2**, 084408 (2018).
- [4] R. Barua, B.T. Lejeune, L. Ke, G. Hadjipanayis, E.M. Levin, R.W. McCallum, M.J. Kramer, and L.H. Lewis, "Anisotropic magnetocaloric response in AlFe_2B_2 ," *Journal of Alloys and Compounds* **745**, 505 – 512 (2018).
- [5] Ping Chai, Sebastian A. Stojan, Xiaoyan Tan, Paul A. Dube, and Michael Shatruk, "Investigation of magnetic properties and electronic structure of layered-structure borides AlT_2B_2 ($T=\text{Fe, Mn, Cr}$) and $\text{AlFe}_{2-x}\text{Mn}_x\text{B}_2$," *Journal of Solid State Chemistry* **224**, 52 – 61 (2015).
- [6] Liqin Ke, Bruce N. Harmon, and Matthew J. Kramer, "Electronic structure and magnetic properties in $T_2\text{AlB}_2$ ($T=\text{Fe, Mn, Cr, Co, and Ni}$) and their alloys," *Phys. Rev. B* **95**, 104427 (2017).
- [7] D. Potashnikov, E.N. Caspi, A. Pesach, A. Hoser, S. Kota, L. Verger, M.W. Barsoum, I. Felner, A. Keren, and O. Rivin, "Magnetic ordering in the nano-laminar ternary Mn_2AlB_2 using neutron and X-ray diffraction," *Journal of Magnetism and Magnetic Materials* **471**, 468 – 474 (2019).
- [8] L. Verger, S. Kota, H. Roussel, T. Ouisse, and M. W. Barsoum, "Anisotropic thermal expansions of select layered ternary transition metal borides: MoAlB , Cr_2AlB_2 , Mn_2AlB_2 , and Fe_2AlB_2 ," *Journal of Applied Physics* **124**, 205108 (2018).
- [9] Kirill D. Belashchenko, Liqin Ke, Markus Dane, Lorin X. Benedict, Tej Nath Lamichhane, Valentin Taufour, Anton Jesche, Sergey L. Bud'ko, Paul C. Canfield, and Vladimir P. Antropov, "Origin of the spin reorientation transitions in $(\text{Fe}_{1-x}\text{Co}_x)_2\text{B}$ alloys," *Applied Physics Letters* **106**, 062408 (2015), <https://doi.org/10.1063/1.4908056>.
- [10] Paul C. Canfield and Ian R. Fisher, "High-temperature solution growth of intermetallic single crystals and quasicrystals," *Journal of Crystal Growth*, 155 – 161 (2001).
- [11] W. R. Meier, T. Kong, S. L. Bud'ko, and P. C. Canfield, "Optimization of the crystal growth of the superconductor $\text{CaKFe}_4\text{As}_4$ from solution in the $\text{FeAs} - \text{CaFe}_2\text{As}_2 - \text{KFe}_2\text{As}_2$ system," *Phys. Rev. Materials* **1**, 013401 (2017).
- [12] Paul C. Canfield, Tai Kong, Udhara S. Kaluarachchi, and Na Hyun Jo, "Use of frit-disc crucibles for routine and exploratory solution growth of single crystalline samples," *Philosophical Magazine* **96**, 84 – 92 (2016).
- [13] Tej N. Lamichhane, Valentin Taufour, Morgan W. Masters, David S. Parker, Udhara S. Kaluarachchi, Srinivasa Thimmaiah, Sergey L. Bud'ko, and Paul C. Canfield, "Discovery of ferromagnetism with large magnetic anisotropy in ZrMnP and HfMnP ," *Applied Physics Letters* **109**, 092402 (2016).
- [14] A. C. Larson and R. B. Von Dreele, "General structure analysis system," Los Alamos National Laboratory Report No. LAUR 86-748 (2004).
- [15] Brian H. Toby, "*EXPGUI*, a graphical user interface for *GSAS*," *Journal of Applied Crystallography* **34**, 210–213 (2001).
- [16] A. Jesche, M. Fix, A. Kreyssig, W. R. Meier, and P. C. Canfield, "X-ray diffraction on large single crystals using a powder diffractometer," *Philosophical Magazine* **96**, 2115–2124 (2016), <https://doi.org/10.1080/14786435.2016.1192725>.
- [17] Michael E. Fisher and J. S. Langer, "Resistive anomalies at magnetic critical points," *Phys. Rev. Lett.* **20**, 665–668 (1968).
- [18] Michael E. Fisher, "Relation between the specific heat and susceptibility of an antiferromagnet," *The Philosophical Magazine: A Journal of Theoretical Experimental and Applied Physics* **7**, 1731–1743 (1962), <https://doi.org/10.1080/14786436208213705>.
- [19] J. Ma, C. D. Dela Cruz, Tao Hong, W. Tian, A. A. Aczel, Songxue Chi, J.-Q. Yan, Z. L. Dun, H. D. Zhou, and M. Matsuda, "Magnetic phase transition in the low-dimensional compound $\text{BaMn}_2\text{Si}_2\text{O}_7$," *Phys. Rev. B* **88**, 144405 (2013).
- [20] A.N Vasil'ev, L.A Ponomarenko, H Manaka, I Yamada, M Isobe, and Y Ueda, "Quasi-one-dimensional antiferromagnetic spinel compound LiCuVO_4 ," *Physica B: Condensed Matter* **284-288**, 1619 – 1620 (2000).
- [21] Y.J. Kim, M. Greven, U.-J. Wiese, and R.J. Birgeneau, "Monte-carlo study of correlations in quantum spin chains at non-zero temperature," *The European Physical Journal B - Condensed Matter and Complex Systems* **4**, 291–297 (1998).
- [22] Jill C. Bonner and Michael E. Fisher, "Linear magnetic chains with anisotropic coupling," *Physical Review* **135**, 640 – 658 (1964).
- [23] R. Dingle, M. E. Lines, and S. L. Holt, "Linear-Chain Antiferromagnetism in $[(\text{CH}_3)_4\text{N}][\text{MnCl}_3]$," *Phys. Rev.* **187**, 643–648 (1969).
- [24] R. Nath, K. M. Ranjith, B. Roy, D. C. Johnston, Y. Furukawa, and A. A. Tsirlin, "Magnetic transitions in the spin- $\frac{5}{2}$ frustrated magnet BiMn_2PO_6 and strong lattice softening in BiMn_2PO_6 and BiZn_2PO_6 below 200 K," *Phys. Rev. B* **90**, 024431 (2014).
- [25] B. Pedrini, J. L. Gavilano, D. Rau, H. R. Ott, S. M. Kazakov, J. Karpinski, and S. Wessel, "NMR and dc susceptibility studies of NaVGe_2O_6 ," *Phys. Rev. B* **70**, 024421 (2004).
- [26] Jun Kikuchi, Kazuhiro Ishiguchi, Kiyochiro Motoya, Masayuki Itoh, Kazunori Inari, Naotoshi Eguchi, and Jun Akimitsu, "NMR and Neutron Scattering Studies of Quasi One-Dimensional Magnet CuV_2O_6 ," *Journal of the Physical Society of Japan* **69**, 2660–2668 (2000).
- [27] Yukiichi Ideta, Yu Kawasaki, Yutaka Kishimoto, Takashi Ohno, Yoshitaka Michihiro, Zhangzhen He, Yutaka Ueda, and Mitsuru Itoh, " ^{51}V NMR study of antiferromagnetic state and spin dynamics in quasi-one-dimensional $\text{BaCo}_2\text{V}_2\text{O}_8$," *Phys. Rev. B* **86**, 094433 (2012).